

---

# Gradient-Based Neural DAG Learning

---

Sébastien Lachapelle<sup>1</sup> Philippe Brouillard<sup>1</sup> Tristan Deleu<sup>1</sup> Simon Lacoste-Julien<sup>1,2</sup>

<sup>1</sup>Mila, Université de Montréal

<sup>2</sup>Canada CIFAR AI Chair

## Abstract

We propose a novel score-based approach to learning a directed acyclic graph (DAG) from observational data. We adapt a recently proposed continuous constrained optimization formulation to allow for nonlinear relationships between variables using neural networks. This extension allows to model complex interactions while being more global in its search compared to other greedy approaches. In addition to comparing our method to existing continuous optimization methods, we provide missing empirical comparisons to nonlinear greedy search methods. On both synthetic and real-world data sets, this new method outperforms current continuous methods on most tasks while being competitive with existing greedy search methods on important metrics for causal inference.

## 1 Introduction

Structure learning and causal inference have many important applications in different areas of science such as genetics [18, 28], biology [30] and economics [21]. *Bayesian networks* (BN), which encode conditional independencies using *directed acyclic graphs* (DAG), are powerful models which are both interpretable and computationally tractable. *Causal graphical models* (CGM) [28] are BNs which support *interventional* queries like: *What will happen if someone external to the system intervene on variable X?* Recent work suggests that causality could partially solve challenges faced by current machine learning systems such as robustness to out-of-distribution samples, adaptability and explainability [22, 20]. However, structure and causal learning are daunting tasks due to both the combinatorial nature of the space of structures and the question of *structure identifiability* (see Section 2.2). Nevertheless, these graphical models known qualities and promises of improvement for machine intelligence renders the quest for structure/causal learning appealing.

In this work, we propose a novel score-based method [18, 28] for structure learning named GraN-DAG which makes use of a recent reformulation of the original *combinatorial problem* of finding an optimal DAG into a *continuous constrained optimization problem*. In the original method named NOTEARS [37], the directed graph is encoded as a *weighted adjacency matrix*  $W$  which represents coefficients in a linear *structural equation model* (SEM) [21] (see Section 2.3). To enforce acyclicity, the authors propose a constraint which is both efficiently computable and easily differentiable. This makes the continuous constrained optimization problem approximately solvable by standard numerical techniques.

Our first contribution is to extend the work of [37] to deal with nonlinear relationships between variables using neural networks (NN) [13]. GraN-DAG is general enough to deal with a large variety of parametric families of conditional probability distributions. To adapt the acyclicity constraint to our nonlinear model, we use an argument similar to what is used in [37] and apply it first at the level of *neural network paths* and then at the level of *graph paths*. Our adapted constraint allows us to exploit the full flexibility of NNs. On both synthetic and real-world tasks, we show GraN-DAG

---

Contact: [sebastien.lachapelle@umontreal.ca](mailto:sebastien.lachapelle@umontreal.ca)

outperforms other approaches which leverage the continuous paradigm, including DAG-GNN [35], a recent nonlinear extension of [37] independently developed which uses an evidence lower bound as score.

Our second contribution is to provide a missing empirical comparison to existing methods that support nonlinear relationships but tackle the optimization problem in its discrete form using greedy search procedures, namely RESIT [27] and CAM [5]. We show that GraN-DAG is competitive on the wide range of tasks we considered.

## 2 Background and related work

Before presenting GraN-DAG, we review concepts relevant to structure and causal learning.

### 2.1 Causal graphical models

We suppose the natural phenomenon of interest can be described by a random vector  $X \in \mathbb{R}^d$  entailed by an underlying CGM  $(P_X, \mathcal{G})$  where  $P_X$  is a probability distribution over  $X$  and  $\mathcal{G} = (V, E)$  is a DAG [28]. Each node  $i \in V$  corresponds to exactly one variable in the system. Let  $\pi_i^{\mathcal{G}}$  denote the set of parents of node  $i$  in  $\mathcal{G}$  and let  $X_{\pi_i^{\mathcal{G}}}$  denote the random vector containing the variables corresponding to the parents of  $i$  in  $\mathcal{G}$ . Throughout the paper, we assume there are no hidden variables. In a CGM, the distribution  $P_X$  is said to be *Markov* to  $\mathcal{G}$  which means we can write the probability density function (pdf) as  $p(x) = \prod_{i=1}^d p_i(x_i | x_{\pi_i^{\mathcal{G}}})$  where  $p_i(x_i | x_{\pi_i^{\mathcal{G}}})$  is the conditional pdf of variable  $X_i$  conditioned on  $X_{\pi_i^{\mathcal{G}}}$ . A CGM can be thought of as a BN in which directed edges are given a causal meaning, allowing it to answer queries regarding *interventional distributions* [18].

### 2.2 Structure identifiability

In general, it is impossible to recover  $\mathcal{G}$  given samples from  $P_X$ . It is, however, customary to rely on a set of assumptions to render the structure fully or partially *identifiable*.

**Definition 1.** Given a set of assumptions  $A$  on a CGM  $\mathcal{M} = (P_X, \mathcal{G})$ , its graph  $\mathcal{G}$  is said to be *identifiable* from  $P_X$  if there exists no other CGM  $\tilde{\mathcal{M}} = (\tilde{P}_X, \tilde{\mathcal{G}})$  satisfying all assumptions in  $A$  such that  $\tilde{\mathcal{G}} \neq \mathcal{G}$  and  $\tilde{P}_X = P_X$ .

There are many examples of graph identifiability results for continuous variables [27, 23, 31, 36] as well as for discrete variables [26]. Those results are obtained by assuming that the conditional pdf  $p_i \forall i$  belongs to a specific parametric family  $\mathcal{P}$ . For example, if one assumes that

$$X_i | X_{\pi_i^{\mathcal{G}}} \sim \mathcal{N}(f_i(X_{\pi_i^{\mathcal{G}}}), \sigma_i^2) \quad \forall i \quad (1)$$

where  $f_i$  is a nonlinear function satisfying some mild regularity conditions, then  $\mathcal{G}$  is identifiable from  $P_X$  (see [27] for the complete theorem and its proof). We will make use of this results in Section 4.

One can consider weaker assumptions such as *faithfulness*. We say  $P_X$  is faithful to  $\mathcal{G}$  when we have that whenever a conditional independence is present in  $P_X$ , its corresponding d-separation is also present in  $\mathcal{G}$  [28]. This assumption allows one to identify, not  $\mathcal{G}$  itself, but the *Markov equivalence class* to which it belongs [32]. A Markov equivalence class is a set of DAGs which encodes exactly the same set of conditional independence statements. Such a class can be characterized by a graphical object named a *completed partially directed acyclic graph* (CPDAG) [18, 28]. Some algorithms we use as baselines in Section 4 outputs only a CPDAG.

### 2.3 NOTEARS: Continuous optimization for structure learning

Structure learning is the problem of learning  $\mathcal{G}$  using a data set of  $n$  samples  $\{x^{(1)}, \dots, x^{(n)}\}$  from  $P_X$ . In Section 5, we review popular score-based methods which embrace the combinatorial nature of the problem via greedy search procedures. We now present the work of [37] which approaches the problem from a continuous optimization perspective.

To cast the combinatorial optimization problem into a continuous constrained one, [37] proposes to encode the graph  $\mathcal{G}$  on  $d$  nodes as a weighted adjacency matrix  $V = [v_1 | \dots | v_d] \in \mathbb{R}^{d \times d}$  which

represents (possibly negative) coefficients in a linear *structural equation model* (SEM) [21] of the form  $X_i := v_i^\top X + N_i \forall i$  where  $N_i$  is a noise variable. Let  $\mathcal{G}_V$  be the directed graph associated with the SEM and let  $A_V$  be the (binary) adjacency matrix associated with  $\mathcal{G}_V$ . One can see that the following equivalence holds:

$$(A_V)_{ij} = 0 \iff V_{ij} = 0 \quad (2)$$

To make sure  $\mathcal{G}_V$  is acyclic, the authors propose the following constraint on  $V$ :

$$\text{Tr } e^{V \odot V} - d = 0 \quad (3)$$

where  $e^M \triangleq \sum_{k=0}^{\infty} \frac{M^k}{k!}$  is the *matrix exponential* and  $\odot$  is the Hadamard product.

To see why this constraint characterizes acyclicity, first note that  $(A_V^k)_{ii}$  is the number of cycles of length  $k$  passing through node  $i$  in graph  $\mathcal{G}_V$ . Clearly, for  $\mathcal{G}_V$  to be acyclic, we must have  $\text{Tr } A_V^k = 0$  for  $k = 1, 2, \dots, \infty$ . By equivalence (2), this is true when  $\text{Tr}(V \odot V)^k = 0$  for  $k = 1, 2, \dots, \infty$ .<sup>2</sup> From there, one can simply apply the definition of the matrix exponential to see why constraint 3 characterizes acyclicity (see [37] for the full development).

The authors propose to use a regularized negative least square score (maximum likelihood for a Gaussian noise model). The resulting continuous constrained problem is

$$\max_V \mathcal{S}(V, \mathbf{X}) \triangleq -\frac{1}{2n} \|\mathbf{X} - \mathbf{X}V\|_F^2 - \lambda \|V\|_1 \quad \text{s.t.} \quad \text{Tr } e^{V \odot V} - d = 0 \quad (4)$$

where  $\mathbf{X} \in \mathbb{R}^{n \times d}$  is the design matrix containing all  $n$  samples. Even though the authors do not discuss explicitly identifiability issues, they point out consistency results for their LS score in [34, 1, 19]. The nature of the problem has been drastically changed: we went from a combinatorial to a continuous problem. The difficulties of combinatorial optimization have been replaced by those of non-convex optimization, since the feasible set is non-convex. Nevertheless, a standard numerical solver for constrained optimization such as an *augmented Lagrangian method* (AL) [4] can be applied to get an approximate solution. The algorithm stops when the constraint is sufficiently close to zero and returns  $\hat{V}$ . Finally, the values of  $\hat{V}$  are thresholded to zero yielding  $\hat{V}_{\text{thresh}}$ .

This method has the advantage of being more global than other approximate greedy methods in the sense that the whole matrix  $W$  is updated at each iteration.<sup>3</sup>

### 3 GraN-DAG: Gradient-based neural DAG learning

We propose a new nonlinear extension to the framework presented in Section 2.3. For each variable  $X_i$ , we learn a fully connected neural network with  $L$  hidden layers parametrized by  $\phi_{(i)} \triangleq \{W_{(i)}^{(1)}, \dots, W_{(i)}^{(L+1)}\}$  where  $W_{(i)}^{(\ell)}$  is the  $\ell$ th weight matrix of the  $i$ th NN.<sup>4</sup> Each NN takes as input  $X_{-i} \in \mathbb{R}^d$ , i.e. the vector  $X$  with the  $i$ th component masked to zero, and outputs  $\theta_{(i)} \in \mathbb{R}^m$ , the  $m$ -dimensional parameter vector of the desired distribution family for variable  $X_i$ .<sup>5</sup> The fully connected NNs have the following form

$$\theta_{(i)} \triangleq W_{(i)}^{(L+1)} g(\dots g(W_{(i)}^{(2)} g(W_{(i)}^{(1)} X_{-i})) \dots) \quad \forall i \quad (5)$$

where  $g$  is a nonlinearity applied element-wise. Note that the evaluation of all NNs can be parallelized on GPU. Distribution families need not be the same for each variable. Let  $\phi \triangleq \{\phi_{(1)}, \dots, \phi_{(d)}\}$  represents all parameters of all  $d$  NNs. Without any constraint on its parameter  $\phi_{(i)}$ , neural network  $i$  models the conditional pdf  $p_i(x_i | x_{-i}; \theta_{(i)})$ . Note that the product  $\prod_{i=1}^d p_i(x_i | x_{-i}; \theta_{(i)})$  is not a valid joint pdf since it does not decompose according to a DAG. We now show how one can constrain  $\phi$  to make sure the product of all conditionals outputted by the NNs is a valid joint pdf. The idea is to define a new weighted adjacency matrix  $A_\phi$  similar to the one encountered in Section 2.3, which can be directly used inside the constraint of Equation 3 to enforce acyclicity.

<sup>2</sup> $V \odot V$  is used instead of  $V$  since some entries might be negative which could yield  $\text{Tr}(V)^k = 0$  for  $k = 1, 2, \dots, \infty$  without having acyclicity.

<sup>3</sup>On the other hand, the update of  $V$  is based on the gradient information of the augmented Lagrangian, which is local in another sense.

<sup>4</sup>We omit biases for clarity.

<sup>5</sup>Not all parameter vectors need to have the same dimensionality, but to simplify the notation, we suppose  $m_i = m \forall i$

### 3.1 Neural network connectivity

Before defining the weighted adjacency matrix  $A_\phi$ , we need to focus on how one can make some NN outputs unaffected by some inputs. Since we will discuss properties of a single NN, we drop the NN subscript ( $i$ ) to improve readability.

We will use the term *neural network path* to refer to a computation path in a NN. For example, in a NN with two hidden layers, the sequence of weights  $(W_{h_1j}^{(1)}, W_{h_2h_1}^{(2)}, W_{kh_2}^{(3)})$  is a NN path from input  $j$  to output  $k$ . We say that a NN path is *inactive* if at least one weight along the path is zero. We can loosely interpret the *path product*  $|W_{h_1j}^{(1)}||W_{h_2h_1}^{(2)}||W_{kh_2}^{(3)}| \geq 0$  as the strength of the NN path, where a path product equal to zero if and only if the path is inactive. Note that if all NN paths from input  $j$  to output  $k$  are inactive (i.e. the sum of their path products is zero), then output  $k$  does not depend on input  $j$  anymore since the information in input  $j$  will never reach output  $k$ . The sum of all path products from every input  $j$  to every output  $k$  can be easily computed by taking the product of all the weight matrices in absolute value.

$$C \triangleq |W^{(L+1)}| \dots |W^{(2)}||W^{(1)}| \in \mathbb{R}_{\geq 0}^{m \times d} \quad (6)$$

where  $|W|$  is the element-wise absolute value of  $W$ . Let us name  $C$  the *neural network connectivity matrix*. It can be verified that  $C_{kj}$  is the sum of all NN path products from input  $j$  to output  $k$ . This means it is sufficient to have  $C_{kj} = 0$  to render output  $k$  independent of input  $j$ .

Remember that each NN in our model outputs a parameter vector  $\theta$  for a conditional distribution and that we want the product of all conditionals to be a valid joint pdf, i.e. we want its corresponding directed graph to be acyclic. With this in mind, we see that it could be useful to make a certain parameter  $\theta$  not dependent on certain inputs of the NN. To have  $\theta$  independent of variable  $X_j$ , it is sufficient to have  $\sum_{k=1}^m C_{kj} = 0$ .

### 3.2 A weighted adjacency matrix

We now define a weighted adjacency matrix  $A_\phi$  that can be used in constraint of Equation 3.

$$(A_\phi)_{ji} \triangleq \begin{cases} \sum_{k=1}^m (C_{(i)})_{kj}, & \text{if } i \neq j \\ 0, & \text{otherwise} \end{cases} \quad (7)$$

where  $C_{(i)}$  denotes the connectivity matrix of the NN associated with variable  $X_i$ .

As the notation suggests,  $A_\phi \in \mathbb{R}_{\geq 0}^{d \times d}$  depends on all weights of all NNs. Moreover, it can effectively be interpreted as a weighted adjacency matrix similarly to what we presented in Section 2.3, since we have that

$$(A_\phi)_{ij} = 0 \implies \theta_{(j)} \text{ does not depend on variable } X_i \quad (8)$$

We note  $\mathcal{G}_\phi$  to be the directed graph entailed by parameter  $\phi$ . We can now write our adapted acyclicity constraint:

$$h(\phi) \triangleq \text{Tr } e^{A_\phi} - d = 0 \quad (9)$$

Note that we can compute the gradient of  $h(\phi)$  w.r.t.  $\phi$  (except on points of non-differentiability arising from the absolute value function, similar to standard neural networks with ReLU activations [12]).

### 3.3 A differentiable score and its optimization

We propose solving the maximum likelihood optimization problem

$$\max_{\phi} \mathbb{E}_{X \sim P_X} \sum_{i=1}^d \log p_i(X_i | X_{\pi_i^\phi}; \theta_{(i)}) \quad \text{s.t.} \quad \text{Tr } e^{A_\phi} - d = 0 \quad (10)$$

where  $\pi_i^\phi$  denotes the set of parents of variable  $i$  in graph  $\mathcal{G}_\phi$ . Note that  $\sum_{i=1}^d \log p_i(X_i | X_{\pi_i^\phi}; \theta_{(i)})$  is a valid log-likelihood function when constraint (9) is satisfied.

As suggested in [37], we apply an augmented Lagrangian approach to get an approximate solution to program (10). Augmented Lagrangian methods consist of optimizing a sequence of subproblems

for which the exact solutions are known to converge to a stationary point of the constrained problem under some regularity conditions [4]. In our case, each subproblem is

$$\max_{\phi} \mathcal{L}(\phi, \lambda_t, \mu_t) \triangleq \mathbb{E}_{X \sim P_X} \sum_{i=1}^d \log p_i(X_i | X_{\pi_i}; \theta_{(i)}) - \lambda_t h(\phi) - \frac{\mu_t}{2} h(\phi)^2 \quad (11)$$

where  $\lambda_t$  and  $\mu_t$  are the Lagrangian and penalty coefficients of the  $t$ th subproblem, respectively. These coefficients are updated after each subproblem is solved. See Appendix A.2 for details regarding the optimization procedure.

### 3.4 Neural networks input masking

Without any masking, the solution outputted by the augmented Lagrangian (AL) will satisfy the constraint only up to numerical precision, i.e. some entries of  $A_\phi$  will be very close to zero. Hence some thresholding is needed. To do so, we mask the inputs of each NN  $i$  using a binary matrix  $M_{(i)} \in \{0, 1\}^{d \times d}$  initialized to have  $(M_{(i)})_{jj} = 1 \ \forall j \neq i$  and zeros everywhere else. Having  $(M_{(i)})_{jj} = 0$  means the input  $j$  of NN  $i$  has been thresholded. This mask is integrated in the product of Equation 6 by doing  $C_{(i)} \triangleq |W_{(i)}^{(L+1)}| \dots |W_{(i)}^{(1)}| M_{(i)}$  without changing the interpretation of  $C_{(i)}$ . During the AL procedure, when a certain entry  $(A_\phi)_{ij}$  is smaller than the threshold  $\epsilon = 10^{-4}$ , the corresponding mask entry is set to zero. The masks  $M_{(i)}$  are never updated via gradient descent. We provide more details on how we ensure the estimated graph  $\mathcal{G}_\phi$  is a DAG in Appendix A.3. The resulting DAG often contains spurious edges, hence we apply a final pruning step identical to what is done in CAM [5]. We provide more details on pruning in Appendix A.4

## 4 Experiments

In this section, we compare GraN-DAG to various baselines (both in the continuous and combinatorial paradigm), namely DAG-GNN [35], NOTEARS [37], RESIT [27] and CAM [5]. Those methods are discussed in Section 5. As a sanity check, we report the performance of random graphs sampled using the *Erdős–Rényi* (ER) scheme described in Appendix A.5 (denoted by RANDOM). For each approach, we evaluate the estimated graph on two metrics: the *structural hamming distance* (SHD) and the *structural interventional distance* (SID) [25]. The former simply counts the number of missing, falsely detected or reversed edges. The latter is especially well suited for causal inference since it counts the number of couples  $(i, j)$  such that the interventional distribution  $p(x_i | do(X_j = \bar{x}))$  would be miscalculated if we were to use the estimated graph to form the parent adjustment set. See Appendix A.7 for more details on SHD and SID. We consider both synthetic and real-world data sets.

Since the performance of GES [6] and PC [32] are almost never on par with the best methods presented in this section, we present their evaluation in Appendix A.6.

The code for all experiments can be found at <https://github.com/kurowasan/GraN-DAG>

### 4.1 Synthetic data

We have generated different *data set types* which vary along three dimensions: number of nodes, level of edge sparsity and graph type. For each data set type, we have sampled 10 data sets of size  $n = 1000$ . We consider two different types of graphs, *Erdős–Rényi* (ER) and *scale-free* (SF) graphs. Both types differ in the way graphs are randomly generated (see Appendix A.5).

Given a data set type, a data set is sampled as follows: First, a ground truth DAG  $\mathcal{G}$  is randomly sampled following either the ER or the SF scheme. Then, the data is generated following  $X_i | X_{\pi_i} \sim \mathcal{N}(f_i(X_{\pi_i}), \sigma_i^2) \ \forall i$  with the functions  $f_i$  independently sampled from a Gaussian process with bandwidth one and  $\sigma_i^2$  sampled uniformly. This setup is especially interesting to consider since, as mentioned in Section 2.2, we know the DAG  $\mathcal{G}$  to be identifiable from the distribution [27]. This ensures that finding the correct DAG via maximum likelihood is not impossible.

In those experiments, each NN learned by GraN-DAG outputs a Gaussian mean  $\hat{\mu}_{(i)}$ , i.e.  $\theta_{(i)} := \hat{\mu}_{(i)} \ \forall i$ . The parameters  $\hat{\sigma}_{(i)}^2$  are learned as well, but do not depend on the parent variables  $X_{\pi_i}$ . Note that the linear method NOTEARS and the nonlinear methods CAM and RESIT all make the correct Gaussian model assumption.

We considered graphs of 10, 20, 50 and 100 nodes. We only present results for 10 and 50 nodes in the main paper since the conclusions do not change with graphs of 20 or 100 nodes (see Appendix A.6 for the additional experiments). We consider graphs of  $d$  and  $4d$  edges (respectively denoted by ER1 and ER4 in the case of ER graphs). Note that RESIT was not applied on data sets of 50 or more variables due to computational reasons (see [27]). For graphs of 50 nodes or more, GraN-DAG performs a *preliminary neighborhood selection* (PNS) similar to what is proposed by CAM [5]. This optional preprocessing step helps reducing overfitting for large graphs (details in Appendix A.1).

Table 1: Results for ER and SF graphs of 10 nodes

	ER1		ER4	
	SHD	SID	SHD	SID
GraN-DAG	1.7±2.5	1.7±3.1	8.3±2.8	21.8±8.9
DAG-GNN	11.4±3.1	37.6±14.4	35.1±1.5	81.9±4.7
NOTEARS	12.2±2.9	36.6±13.1	32.6±3.2	79.0±4.1
CAM	1.1±1.1	1.1±2.4	12.2±2.7	30.9±13.2
RESIT	21.1±4.4	19.4±16.4	17.3±3.1	45.2±8.6
RANDOM	26.3±9.8	25.8±10.4	31.8±5.0	76.6±7.0
	SF1		SF4	
	SHD	SID	SHD	SID
GraN-DAG	1.2±1.1	4.1±6.1	9.9±4.0	16.4±6.0
DAG-GNN	9.9±1.1	29.7±15.8	20.8±1.9	48.4±15.6
NOTEARS	10.7±2.2	32.0±15.3	20.8±2.7	49.8±15.6
CAM	1.4±1.6	5.4±6.1	9.8±4.3	19.3±7.5
RESIT	21.8±7.5	11.9±13.7	15.5±9.4	20.4±19.3
RANDOM	25.1±10.2	24.5±10.5	28.5±4.0	47.2±12.2

Table 2: Results for ER and SF graphs of 50 nodes

	ER1		ER4	
	SHD	SID	SHD	SID
GraN-DAG	5.1±2.8	22.4±17.8	102.6±21.2	1060.1±109.4
DAG-GNN	49.2±7.9	304.4±105.1	191.9±15.2	2146.2±64
NOTEARS	62.8±9.2	327.3±119.9	202.3±14.3	2149.1±76.3
CAM	4.3±1.9	22.0±17.9	98.8±20.7	1197.2±125.9
RANDOM	535.7±401.2	272.3±125.5	708.4±234.4	1921.3±203.5
	SF1		SF4	
	SHD	SID	SHD	SID
GraN-DAG	25.5±6.2	90.0±18.9	111.3±12.3	271.2±65.4
DAG-GNN	49.8±1.3	182.8±42.9	144.9±13.3	540.8±151.1
NOTEARS	57.7±3.5	195.7±54.9	153.7±11.8	558.4±153.5
CAM	24.1±6.2	85.7±31.9	111.2±13.3	320.7±152.6
RANDOM	514.0±360.0	381.3±190.3	660.6±194.9	1198.9±304.6

We now examine the different metrics reported in Tables 1 and 2 (the errors bars represent the standard deviation across datasets per task). We can see that, across all settings, GraN-DAG and CAM are the best performing methods, both in terms of SHD and SID. It is not surprising that a linear method such as NOTEARS performs poorly on nonlinear data. What is maybe more surprising is the poor performance of DAG-GNN in terms of SID. It performs similarly to RANDOM in almost all cases except in scale-free networks of 50 nodes or more. In terms of SHD, it performs rarely better than NOTEARS, both on ER and SF. We hypothesize that DAG-GNN performs poorly in our setup because it does not do the correct modelling assumptions and because its architecture uses a strong form of parameter sharing between the functions  $f_i$ , which is not justified in a setup like ours.



Among the continuous approaches considered, GraN-DAG is the best performing on all our synthetic tasks.

Even though CAM (wrongly) assumes that the functions  $f_i$  are additive, i.e.  $f_i(x_{\pi_i^{\mathcal{G}}}) = \sum_{j \in \pi_i^{\mathcal{G}}} f_{ij}(x_j) \forall i$ , it manages to outperform RESIT which does not make this incorrect modelling assumption. This confirms the empirical findings of [5]. On all the synthetic tasks, GraN-DAG is on par with CAM, indicating that pursuing the continuous paradigm for structure learning is worthwhile.

## 4.2 Real data

We have tested all methods considered so far on a well known data set which measures the expression level of different proteins and phospholipids in human cells [30]. This data set contains both *observational* and *interventional* data [18, 28]. Since this paper focuses on learning structures from purely observational data, we omit interventional data, which yields  $n = 853$  samples. This dataset and its ground truth graph proposed in [30] are often used in the probabilistic graphical model literature [18]. The graph has  $d = 11$  nodes and 17 edges.

Note that in this application, it is not clear whether the DAG  $\mathcal{G}$  is identifiable from the distribution. Nevertheless, we apply procedures to estimate it. This departure from identifiable setups is an occasion to explore different modelling assumptions for GraN-DAG. In addition to the model presented in Section 4.1, we consider an alternative, denoted GraN-DAG++, which allows the variance parameters  $\hat{\sigma}_{(i)}^2$  to depend on the parent variables  $X_{\pi_i^{\mathcal{G}}}$  through the NN, i.e.  $\theta_{(i)} := (\hat{\mu}_{(i)}, \log \hat{\sigma}_{(i)}^2)$ . This allows the model to capture heteroscedastic noise.

In addition to metrics used in Section 4.1, we also report SHD-CPDAG. To compute the SHD-CPDAG between two DAGs, we first map each of them to their corresponding CPDAG and measure the SHD between the two. This metric is useful to compare algorithms which only outputs a CPDAG like GES and PC to other methods which outputs a DAG. Note also that, for these methods, we report an approximate lower bound and upper bound on the SID. This is necessary since the SID can only be measured on DAGs (see A.7 for more details on all metrics). Results are reported in Table 3.

Table 3: Results on protein signaling data set

	SHD	SHD-CPDAG	SID
GraN-DAG	13	11	47
GraN-DAG++	13	10	48
DAG-GNN	16	21	44
NOTEARS	21	21	44
CAM	12	9	55
RESIT	27	22	57
GES	26	28	[34, 45]
PC	17	11	[47, 62]
RANDOM	21	20	60

A first observation is that, both in terms of SID and SHD, all methods perform worse than what was reported for graphs of similar size in Section 4.1. This might be due to the lack of identifiability guarantees we face in applications. Nevertheless, all methods except GES and NOTEARS score better than RANDOM on all three metrics. Both GraN-DAG experiments outperform CAM in terms of SID (which differs from the general trend of Section 4.1) and arrive almost on par in terms of SHD and SHD-CPDAG. This time, DAG-GNN and NOTEARS outperform both CAM and GraN-DAG on SID, but not on SHD and SHD-CPDAG. In terms of SHD-CPDAG, PC is among the best. The low SHD-CPDAG for GraN-DAG and CAM indicates that such methods can be used to identify Markov equivalence classes, although their main purpose is to estimate DAGs.

## 5 Related Work

Most methods for structure learning from observational data make use of some identifiability results similar to the ones raised in Section 2.2. Roughly speaking, there are two classes of methods: *independence-based* and *score-based* methods. GraN-DAG falls into the second class.

Independence-based methods such as PC [32] assume  $P_X$  is faithful to  $\mathcal{G}$  and relies on statistical conditional independence tests (e.g. based on HSIC [15]) to recover the underlying CPDAG. One can also deal with hidden variables with FCI [32], a modified version of PC.

Score-based methods [18, 28] cast the problem of structure learning as an optimization problem over the space of structures (it can either be the space of DAGs or CPDAGs). Many popular algorithms tackle the combinatorial nature of the problem by performing a form of greedy search. GES [6] is a popular example. It usually assumes a linear parametric model with Gaussian noise and greedily search the space of CPDAGs in order to optimize the Bayesian information criterion. Other greedy approaches rely on parametric assumptions which render  $\mathcal{G}$  fully identifiable. For example, [23] relies on a linear Gaussian model with equal variances to render the DAG identifiable. RESIT [27], assumes nonlinear relationships with additive Gaussian noise and greedily maximizes an independence-based score. CAM [5] decouples the search for the optimal node ordering from the parents selection for each node. Moreover, CAM assumes an additive noise model (ANM) [28] in which the nonlinear functions are additive, which provides a computational advantage when searching over the space of DAGs. As mentioned in Section 2.3, NOTEARS, proposed in [37], tackles the problem of finding an optimal DAG as a continuous constrained optimization program. This is a drastic departure from previous combinatorial approaches which enables the application of well studied numerical solvers for continuous optimizations. Recent independent work proposes DAG-GNN [35], a graph neural network architecture which can be used to learn DAGs via the maximization of an evidence lower bound (ELBO). To the best of our knowledge, DAG-GNN is the first approach extending the work of [37] for structure learning supporting nonlinear relationships. Although [35] provides empirical comparisons to linear approaches, namely NOTEARS and FGS (a faster extension of GES) [29], comparisons to known greedy approaches supporting nonlinear relationships such as RESIT and CAM are missing. There exists certain score-based approaches which uses integer linear programming (ILP) [16, 8] which internally solve continuous linear relaxations. Connections between such methods and the continuous constrained approaches are to be explored.

Methods for causal discovery using NNs have already been proposed. SAM [17] learns conditional NN generators using adversarial losses but does not enforce acyclicity. CGNN [14], when used for multivariate data, requires an initial skeleton to learn the different functional relationships.

GraN-DAG has strong connections with MADE [9], a method used to learn distributions using a masked NN which enforce the so-called *autoregressive property*. The autoregressive property and acyclicity are in fact equivalent. MADE does not learn the weight masking, it fixes it at the beginning of the procedure. GraN-DAG could be used with a unique NN taking as input all variables and outputting parameters for all conditional distributions. In this case, it would be similar to MADE, except the variable ordering would be learned from data instead of fixed *a priori*.

## 6 Conclusion

The continuous constrained approach to structure learning has the advantage of being more global than other approximate greedy methods and allows to replace task-specific greedy algorithms by appropriate off-the-shelf numerical solvers. In this work, we have introduced GraN-DAG, a novel score-based approach for structure learning supporting nonlinear relationships while leveraging a continuous optimization paradigm. The method rests on an acyclicity constraint very similar to the one proposed in [37] where the weighted adjacency matrix is adapted to deal with fully connected NNs instead of linear functions. We showed GraN-DAG outperforms other gradient-based approaches, namely NOTEARS and its recent nonlinear extension DAG-GNN, on the synthetic data sets considered in Section 4.1 while being competitive on the protein expression levels data set of Section 4.2. Compared to greedy approaches, GraN-DAG is competitive across all datasets considered. To the best of our knowledge, GraN-DAG is the first approach leveraging the continuous paradigm introduced in [37] which has been shown to be competitive with state of the art combinatorial approaches supporting nonlinear relationships.



## Acknowledgments

This research was partially supported by the Canada CIFAR AI Chair Program and by a Google Focused Research award. The authors would like to thank Rémi Le Priol, Tatjana Chavdarova, Charles Guille-Escuret and Yoshua Bengio for insightful discussions as well as Florian Bordes for technical support.

## References

- [1] B. Aragam, A.A. Amini, and Q. Zhou. Learning directed acyclic graphs with penalized neighbourhood regression. *arXiv preprint arXiv:1511.08963*, 2015.
- [2] A.-L. Barabási. Scale-free networks: a decade and beyond. *Science*, 2009.
- [3] A.-L. Barabási and R. Albert. Emergence of scaling in random networks. *Science*, 1999.
- [4] D.P. Bertsekas. *Nonlinear Programming*. Athena Scientific, 1999.
- [5] P. Bühlmann, J. Peters, and J. Ernest. CAM: Causal additive models, high-dimensional order search and penalized regression. *Annals of Statistics*, 2014.
- [6] D.M. Chickering. Optimal structure identification with greedy search. *Journal of Machine Learning Research*, 2003.
- [7] A. Clauset, C.R. Shalizi, and M.E.J. Newman. Power-law distributions in empirical data. *SIAM review*, 2009.
- [8] J. Cussens. Bayesian network learning with cutting planes. In *Proceedings of the 27th Conference on Uncertainty in Artificial Intelligence*, 2011.
- [9] M. Germain, K. Gregor, I. Murray, and H. Larochelle. Made: Masked autoencoder for distribution estimation. In *Proceedings of the 32nd International Conference on Machine Learning*, 2015.
- [10] P. Geurts, D. Ernst, and L. Wehenkel. Extremely randomized trees. *Machine learning*, 2006.
- [11] X. Glorot and Y. Bengio. Understanding the difficulty of training deep feedforward neural networks. In *Proceedings of the 13th International Conference on Artificial Intelligence and Statistics*, 2010.
- [12] X. Glorot, A. Bordes, and Y. Bengio. Deep sparse rectifier neural networks. In *Proceedings of the 14th International Conference on Artificial Intelligence and Statistics*, 2011.
- [13] I. Goodfellow, Y. Bengio, and A. Courville. *Deep Learning*. MIT Press, 2016.
- [14] O. Goudet, D. Kalainathan, P. Caillou, D. Lopez-Paz, I. Guyon, and M. Sebag. Learning Functional Causal Models with Generative Neural Networks. In *Explainable and Interpretable Models in Computer Vision and Machine Learning*. Springer International Publishing, 2018.
- [15] A. Gretton, K. Fukumizu, C.H. Teo, L. Song, B. Schölkopf, and A.J. Smola. A kernel statistical test of independence. In *Advances in neural information processing systems 20*, 2007.
- [16] T. Jaakkola, D. Sontag, A. Globerson, and M. Meila. Learning Bayesian Network Structure using LP Relaxations. In *Proceedings of the 13th International Conference on Artificial Intelligence and Statistics*, 2010.
- [17] D. Kalainathan, O. Goudet, I. Guyon, D. Lopez-Paz, and M. Sebag. Sam: Structural agnostic model, causal discovery and penalized adversarial learning. *arXiv preprint arXiv:1803.04929*, 2018.
- [18] D. Koller and N. Friedman. *Probabilistic Graphical Models: Principles and Techniques - Adaptive Computation and Machine Learning*. MIT Press, 2009.
- [19] P.-L. Loh and P. Bühlmann. High-dimensional learning of linear causal networks via inverse covariance estimation. *Journal of Machine Learning Research*, 2014.

- [20] S. Magliacane, T. van Ommen, T. Claassen, S. Bongers, P. Versteeg, and J.M. Mooij. Domain adaptation by using causal inference to predict invariant conditional distributions. In *Advances in Neural Information Processing Systems 31*, 2018.
- [21] J. Pearl. *Causality: Models, Reasoning and Inference*. Cambridge University Press, 2nd edition, 2009.
- [22] J. Pearl. The seven tools of causal inference, with reflections on machine learning. *Commun. ACM*, 2019.
- [23] J. Peters and P. Bühlman. Identifiability of Gaussian structural equation models with equal error variances. *Biometrika*, 2014.
- [24] J. Peters and P. Bühlmann. Structural intervention distance (SID) for evaluating causal graphs. *Neural Computation*, 2015.
- [25] J. Peters and P. Bühlmann. Structural intervention distance (sid) for evaluating causal graphs. *Neural Computation*, 2013.
- [26] J. Peters, D. Janzing, and B. Schölkopf. Causal inference on discrete data using additive noise models. *IEEE Transactions on Pattern Analysis and Machine Intelligence*, 2011.
- [27] J. Peters, J. M. Mooij, D. Janzing, and B. Schölkopf. Causal discovery with continuous additive noise models. *Journal of Machine Learning Research*, 2014.
- [28] J. Peters, D. Janzing, and B. Schölkopf. *Elements of Causal Inference - Foundations and Learning Algorithms*. MIT Press, 2017.
- [29] J. Ramsey, M. Glymour, R. Sanchez-Romero, and C. Glymour. A million variables and more: the fast greedy equivalence search algorithm for learning high-dimensional graphical causal models, with an application to functional magnetic resonance images. *I. J. Data Science and Analytics*, 2017.
- [30] K. Sachs, O. Perez, D. Pe’er, D.A. Lauffenburger, and G.P. Nolan. Causal protein-signaling networks derived from multiparameter single-cell data. *Science*, 2005.
- [31] S. Shimizu, P.O. Hoyer, A. Hyvärinen, and A. Kerminen. A linear non-gaussian acyclic model for causal discovery. *Journal of Machine Learning Research*, 2006.
- [32] P. Spirtes, C. Glymour, and R. Scheines. *Causation, Prediction, and Search*. MIT press, 2000.
- [33] T. Tieleman and G. Hinton. Lecture 6.5—RmsProp: Divide the gradient by a running average of its recent magnitude. COURSERA: Neural Networks for Machine Learning, 2012.
- [34] S. van de Geer and P. Bühlmann.  $\ell_0$ -penalized maximum likelihood for sparse directed acyclic graphs. *Annals of Statistics*, 2012.
- [35] Y. Yu, J. Chen, T. Gao, and M. Yu. DAG-GNN: DAG structure learning with graph neural networks. In *Proceedings of the 36th International Conference on Machine Learning*, 2019.
- [36] K. Zhang and A. Hyvärinen. On the identifiability of the post-nonlinear causal model. In *Proceedings of the 25th Conference on Uncertainty in Artificial Intelligence*, 2009.
- [37] X. Zheng, B. Aragam, P.K. Ravikumar, and E.P. Xing. Dags with no tears: Continuous optimization for structure learning. In *Advances in Neural Information Processing Systems 31*, 2018.

## A Appendix

### A.1 Preliminary neighborhood selection

For graphs of 50 nodes or more, GraN-DAG performs a *preliminary neighborhood selection* (PNS) similar to what has been proposed in [5]. This procedure applies a variable selection method to get a set of possible parents for each node. This is done by fitting an *extremely randomized trees* [10] (using `ExtraTreesRegressor` from `scikit-learn`) for each variable against all the other variables. For each node a feature importance score based on the gain of purity is calculated. Only nodes that have a feature importance score higher than  $0.75 \cdot \text{mean}$  are kept as potential parent, where  $\text{mean}$  is the mean of the feature importance scores of all nodes. Although the use of PNS in CAM was motivated by gains in computation time, GraN-DAG uses it to avoid overfitting, without reducing the computation time.

### A.2 Optimization

Let us recall the augmented Lagrangian:

$$\max_{\phi} \mathcal{L}(\phi, \lambda_t, \mu_t) \triangleq \mathbb{E}_{X \sim P_X} \sum_{i=1}^d \log p_i(X_i | X_{\pi_i^{\phi}}; \theta_{(i)}) - \lambda_t h(\phi) - \frac{\mu_t}{2} h(\phi)^2 \quad (12)$$

where  $\lambda_t$  and  $\mu_t$  are the Lagrangian and penalty coefficients of the  $t$ th subproblem, respectively. In all our experiments, we initialize those coefficients using  $\lambda_0 = 0$  and  $\mu_0 = 10^{-3}$ . We approximately solve each non-convex subproblem using RMSprop [33], a stochastic gradient descent variant popular for NNs. We use the following gradient estimate:

$$\begin{aligned} \nabla_{\phi} \mathcal{L}(\phi, \lambda_t, \mu_t) &\approx \nabla_{\phi} \hat{\mathcal{L}}_B(\phi, \lambda_t, \mu_t) \\ \text{with } \hat{\mathcal{L}}_B(\phi, \lambda_t, \mu_t) &\triangleq \frac{1}{|B|} \sum_{x \in B} \sum_{i=1}^d \log p_i(x_i | x_{\pi_i^{\phi}}; \theta_{(i)}) - \lambda_t h(\phi) - \frac{\mu_t}{2} h(\phi)^2 \end{aligned} \quad (13)$$

where  $B$  is a minibatch sampled from the data set and  $|B|$  is the minibatch size. The gradient estimate  $\nabla_{\phi} \hat{\mathcal{L}}_B(\phi, \lambda_t, \mu_t)$  can be computed using standard deep learning libraries. We consider a subproblem has converged when  $\hat{\mathcal{L}}_H(\phi, \lambda_t, \mu_t)$  evaluated on a held-out data set  $H$  stops increasing. Let  $\phi_t^*$  be the approximate solution to subproblem  $t$ . Then,  $\lambda_t$  and  $\mu_t$  are updated according to the following rule:

$$\begin{aligned} \lambda_{t+1} &\leftarrow \lambda_t + \mu_t h(\phi_t^*) \\ \mu_{t+1} &\leftarrow \begin{cases} \eta \mu_t, & \text{if } h(\phi_t^*) > \gamma h(\phi_{t-1}^*) \\ \mu_t, & \text{otherwise} \end{cases} \end{aligned} \quad (14)$$

with  $\eta = 10$  and  $\gamma = 0.9$ . Each subproblem  $t$  is initialized using the previous subproblem solution  $\phi_{t-1}^*$ . The augmented Lagrangian method stops when  $h(\phi) \leq 10^{-8}$ .

### A.3 Thresholding

The augmented Lagrangian outputs  $\phi_T^*$  where  $T$  is the number of subproblems solved before declaring convergence. Note that the weighted adjacency matrix  $A_{\phi_T^*}$  will most likely not represent an acyclic graph, even if we threshold as we learn, as explained in Section 3.4. We need to remove additional edges to obtain a DAG (edges are removed using the mask presented in Section 3.4). One option would be to remove edges one by one until a DAG is obtained, starting from the edge  $(i, j)$  with the lowest  $(A_{\phi_T^*})_{ij}$  up to the edge with the highest  $(A_{\phi_T^*})_{ij}$ . This amounts to gradually increasing the threshold  $\epsilon$  until  $A_{\phi_T^*}$  is acyclic. However, this approach has the following flaw: It is possible to have  $(A_{\phi_T^*})_{ij}$  significantly higher than zero while having  $\theta_{(j)}$  almost completely independent of variable  $X_i$ . This can happen for at least two reasons. First, the NN paths from input  $i$  to output  $k$  might end up cancelling each others, rendering the input  $i$  inactive. Second, some neurons of the NNs might always be saturated for the observed range of inputs, rendering some NN paths *effectively inactive* without being inactive in the sense described in Section 3.1. Those two observations illustrate the fact that having  $(A_{\phi_T^*})_{ij} = 0$  is only a sufficient condition to have  $\theta_{(j)}$  independent of variable  $X_i$  and not a necessary one.

To avoid this issue, we consider the following alternative. Consider the function  $\mathcal{L} : \mathbb{R}^d \mapsto \mathbb{R}^d$  which maps all  $d$  variables to their respective conditional likelihoods, i.e.  $\mathcal{L}_i(X) \triangleq p_i(X_i | X_{\pi_i^*}) \forall i$ . We consider the following expected Jacobian matrix

$$\mathcal{J} \triangleq \mathbb{E}_{X \sim P_X} \left| \frac{\partial \mathcal{L}}{\partial X} \right|^\top \quad (15)$$

where  $\left| \frac{\partial \mathcal{L}}{\partial X} \right|$  is the Jacobian matrix of  $\mathcal{L}$  evaluated at  $X$ , in absolute value (element-wise). Similarly to  $(A_{\phi_T^*})_{ij}$ , the entry  $\mathcal{J}_{ij}$  can be loosely interpreted as the strength of edge  $(i, j)$ . We propose removing edges starting from the lowest  $\mathcal{J}_{ij}$  to the highest, stopping as soon as acyclicity is achieved. We believe  $\mathcal{J}$  is better than  $A_{\phi_T^*}$  at capturing which NN inputs are effectively inactive since it takes into account NN paths cancelling each others and saturated neurons. Empirically, we found that using  $\mathcal{J}$  instead of  $A_{\phi_T^*}$  yields better results.

#### A.4 DAG Pruning

Once the thresholding is performed and a DAG is obtained, GraN-DAG performs a pruning step identical to CAM [5] in order to remove spurious edges. We use the implementation of [5] based on the R function `gamboost` from the `mboost` package. For each variable  $X_i$ , a generalized additive model is fitted against the current parents of  $X_i$  and a significance test of covariance is applied. Parents with a p-value higher than 0.001 are removed from the parent set. Similarly to what [5] observed, this pruning phase generally has the effect of greatly reducing the SHD without considerably changing the SID.

#### A.5 Graph types

*Erdős–Rényi* (ER) graphs are generated by randomly sampling a topological order and by adding directed edges were it is allowed independently with probability  $p = \frac{2e}{d^2-d}$  were  $e$  is the expected number of edges in the resulting DAG.

*Scale-free* (SF) graphs were generated using the Barabási–Albert model [3] which is based on preferential attachment. Nodes are added one by one. Between the new node and the existing nodes,  $m$  edges (where  $m$  is equal to  $d$  or  $4d$ ) will be added. An existing node  $i$  have the probability  $p(k_i) = \frac{k_i}{\sum_j k_j}$  to be chosen, where  $k_i$  represents the degree of the node  $i$ . While ER graphs have a degree distribution following a Poisson distribution, SF graphs have a degree distribution following a power law: few nodes, often called *hubs*, have a high degree. Some authors [2] have stated that these types of graphs have similar properties to real-world networks which can be found in many different fields, although these claims remain controversial [7].

#### A.6 Supplementary experiments

The results for 20 and 100 nodes are presented in Table 4 and 5 using exactly the same setting as in Section 4. The conclusions drawn remain the same as for 10 and 50 nodes. For GES and PC, the SHD and SID are respectively presented in Table 6 and 7. Figure A.6 shows the entries of the weighted adjacency matrix  $A_\phi$  as training proceeds in a typical run for 10 nodes.

Table 4: Results for ER and SF graphs of 20 nodes

	ER1		ER4	
	SHD	SID	SHD	SID
GraN-DAG	4.0 ±3.4	17.9±19.5	45.2±10.7	165.1±21.0
DAG-GNN	25.6±7.5	109.1±53.1	75.0±7.7	344.8±17.0
NOTEARS	30.3±7.8	107.3±47.6	79.0±8.0	346.6±13.2
CAM	2.7±1.8	10.6±8.6	41.0±11.9	157.9±41.2
RESIT	134.7±16.9	39.7±31.4	99.2±23.0	185.1±41.7
RANDOM	103.0±39.6	94.3±53.0	117.5±25.9	298.5±28.7
	SF1		SF4	
	SHD	SID	SHD	SID
GraN-DAG	7.6±2.5	28.8±10.4	36.8±5.1	62.5±18.8
DAG-GNN	19.5±1.8	60.1±12.8	49.5±5.4	115.2±33.3
NOTEARS	23.9±3.5	69.4±19.7	52.0±4.5	120.5±32.5
CAM	5.7±2.6	23.3±18.0	35.6±4.5	59.1±18.8
RESIT	137.4±22.0	71.8±38.3	119.4±7.5	98.6±33.0
RANDOM	105.2±48.8	81.1±54.4	121.5±28.5	204.8±38.5

Table 5: Results for ER and SF graphs of 100 nodes

	ER1		ER4	
	SHD	SID	SHD	SID
GraN-DAG	15.1±6.0	83.9±46.0	206.6±31.5	4207.3±419.7
DAG-GNN	110.2±10.5	883.0±320.9	379.5±24.7	8036.1±656.2
NOTEARS	125.6±12.1	913.1±343.8	387.8±25.3	8124.7±577.4
CAM	17.3±4.5	124.9±65.0	186.4±28.8	4601.9±482.7
RANDOM	1561.6±1133.4	1175.3±547.9	2380.9±1458.0	7729.7±1056.0
	SF1		SF4	
	SHD	SID	SHD	SID
GraN-DAG	59.2±7.7	265.4±64.2	262.7±19.6	872.0±130.4
DAG-GNN	97.6±1.5	438.6±112.7	316.0±14.3	1394.6±165.9
NOTEARS	111.7±5.4	484.3±138.4	327.2±15.8	1442.8±210.1
CAM	52.7±9.3	230.3±36.9	255.6±21.7	845.8±161.3
RANDOM	2222.2±1141.2	1164.2±593.3	2485.0±1403.9	4206.4±1642.1

Table 6: SHD for GES and PC

	10 nodes		20 nodes		50 nodes		100 nodes	
	ER1	ER4	ER1	ER4	ER1	ER4	ER1	ER4
GES	13.8±4.8	32.3±4.3	43.3±12.4	94.6±9.8	106.6±24.7	254.4±39.3	292.9±33.6	542.6±51.2
PC	8.4±3	34±2.6	20.1±6.5	73.1±5.8	44.0±11.6	183.6±20	95.2±9.1	358.8±20.6
	SF1		SF4		SF1		SF4	
	SF1	SF4	SF1	SF4	SF1	SF4	SF1	SF4
GES	8.1±2.4	17.4±4.5	26.2±7.5	50.7±6.2	73.9±7.4	178.8±16.5	190.3±22	408.7±24.9
PC	4.8±2.4	16.4±2.8	13.6±2.1	44.4±4.6	43.1±5.7	135.4±10.7	97.6±6.6	314.2±17.5

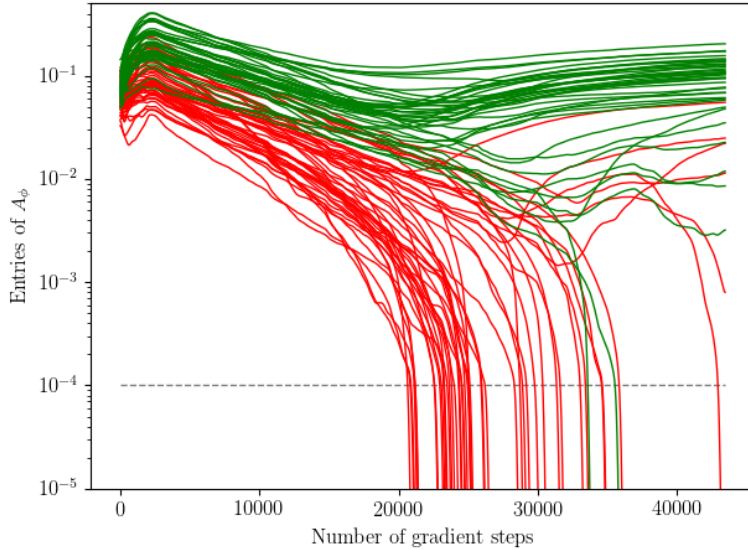


Figure 1: Entries of the weighted adjacency matrix  $A_\phi$  as training proceeds in GraN-DAG for a synthetic data set ER4 with 10 nodes. Green curves represent edges which appear in the ground truth graph while red ones represent edges which do not. The horizontal dashed line at  $10^{-4}$  is the threshold  $\epsilon$  introduced in Section 3.4. We can see that GraN-DAG successfully recovers most edges correctly while keeping few spurious edges.

Table 7: Lower and upper bound on the SID for GES and PC. See Appendix A.7 for details on how to compute SID for CPDAGs.

	10 nodes		20 nodes		50 nodes		100 nodes	
	ER1	ER4	ER1	ER4	ER1	ER4	ER1	ER4
GES	24.1±17.3	68.5±10.5	62.1±44	301.9±19.4	150.9±72.7	1996.6±73.1	582.5±391.1	8054±524.8
	27.2±17.5	75±7	65.7±44.5	319.3±13.3	155.1±74	2032.9±88.7	598.9±408.6	8124.2±470.2
PC	22.6±15.5	78.1±7.4	80.9±51.1	316.7±25.7	222.7±138	2167.9±88.4	620.7±240.9	8236.9±478.5
	27.3±13.1	79.2±5.7	94.9±46.1	328.7±25.6	256.7±127.3	2178.8±80.8	702.5±255.8	8265.4±470.2
	SF1	SF4	SF1	SF4	SF1	SF4	SF1	SF4
GES	11.6±9.2	39.3±11.2	54.9±23.1	89.5±38.4	171.6±70.1	496.3±154.1	511.5±257.6	1421.7±247.4
	16.4±11.7	43.9±14.9	57.9±24.6	105.1±44.3	182.7±77	529.7±184.5	524±252.2	1485.4±233.6
PC	8.3±4.6	36.5±6.2	42.2±14	95.6±37	124.2±38.3	453.2±115.9	414.5±124.4	1369.2±259.9
	16.8±12.3	41.7±6.9	59.7±14.9	118.5±30	167.1±41.4	538±143.7	486.5±120.9	1513.7±296.2

## A.7 Metrics

SHD takes two partially directed acyclic graphs (PDAG) and counts the number of edge for which the edge type differs in both PDAGs. There are four edge types:  $i \leftarrow j$ ,  $i \rightarrow j$ ,  $i - j$  and  $i \cdot j$ . Since this distance is defined over the space of PDAGs, we can use it to compare DAGs with DAGs, DAGs with CPDAGs and CPDAGs with CPDAGs. When comparing a DAG with a CPDAG, having  $i \leftarrow j$  instead of  $i - j$  counts as a mistake.

SHD-CPDAG is very similar to SHD. The only difference is that both DAGs are first mapped to their respective CPDAGs before measuring the SHD.

Introduced in [24], SID counts the number of interventional distribution of the form  $p(x_i | do(x_j = \hat{x}_j))$  that would be miscalculated using the *parent adjustment formula* [21] if we were to use the predicted DAG instead of the ground truth DAG to form the parent adjustment set. Some care needs to be taken to evaluate the SID for methods outputting a CPDAG such as GES and PC. [24] proposes to report the SID of the DAGs which have approximately the minimal and the maximal SID in the Markov equivalence class given by the CPDAG. See [24] for more details.



## A.8 Hyperparameters

All GraN-DAG runs were performed using the following set of hyperparameters. We used RMSprop as optimizer with learning rate of  $10^{-2}$  for the first subproblem and  $10^{-4}$  for all subsequent subproblems. Each NN has two hidden layers with 10 units (except for real-data experiments which uses only 1 hidden layer). Leaky-ReLU is used as activation functions. The NN are initialized using the initialization scheme proposed in [11] also known as *Xavier initialization*. We used minibatches of 64 samples.

For RESIT, we used the default hyperparameters found in the code available on the authors webpages. For NOTEARS and DAG-GNN, we also used the default hyperparameters found in the authors code. For GES and PC, we used default hyperparameters of the `pca1g` R package. For CAM, we used the the default hyperparameters found in the `CAM` R package, with default PNS and DAG pruning.